Effect of RF coil excitation on field inhomogeneity at ultra high fields: A field optimized TEM resonator

Tamer S. Ibrahim[a,b], Robert Lee[b], Brian A. Baertlein[b], Amir M. Abduljalil[a], Hui Zhu[a], Pierre-Marie L. Robitaille[a,*]

[a]*Department of Radiology, The Ohio State University, Columbus, Ohio 43210 USA*
[b]*Department of Electrical Engineering, The Ohio State University, Columbus, Ohio 43210 USA*

Abstract

In this work, computational methods were utilized to optimize the field produced by the transverse electromagnetic (TEM) resonator in the presence of the human head at 8 Tesla. Optimization was achieved through the use of the classical finite difference time domain (FDTD) method and a TEM resonator loaded with an anatomically detailed human head model with a resolution of 2 mm × 2 mm × 2 mm. The head model was developed from 3D MR images. To account for the electromagnetic interactions between the coil and the tissue, the coil and the head were treated as a single system at all the steps of the model including, numerical tuning and excitation. In addition to 2, 3, 4, 6, and 10-port excitations, an antenna array concept was utilized by driving all the possible ports (24) of a 24-strut TEM resonator. The results show that significant improvement in the circularly polarized component of the transverse magnetic field could be obtained when using multiple ports and variable phase and fixed magnitude, or variable phase and variable magnitude excitations. © 2001 Elsevier Science Inc. All rights reserved.

Keywords: TEM Resonator; B_1 field; Numerical optimization; Ultra high field

1. Introduction

In high field (>4 Tesla) MRI systems, a major challenge is the design of RF coils that exhibit a good signal to noise ratio, transverse magnetic (B_1) field uniformity, and low specific absorption rate (SAR) in the biological tissues. Since the Larmor frequency increases linearly with the static magnetic field (B_0), the operational wavelength decreases. Consequently, the wavelength inside the human head and body are comparable. For instance, at 7 Tesla (300 MHz) the wavelength inside the head (average relative dielectric constant of 64) is approximately 12.5 cm. As a result, the largest dimension of the head is about twice the operational wavelength. Given that the human head is asymmetric, and contains highly inhomogeneous, lossy materials, very strong electromagnetic interactions are expected between the RF coil, the excitation source(s) and the head [1,2]. These interactions can lead to a nonuniform, asymmetric, and complex current distributions on the RF coil struts [3,4], which in return produces a nonuniform, circularly polarized B_1 field in the human head.

In order to recover the field homogeneity, the field distribution within the RF coil must be modified. Several approaches have been proposed to accomplish this task. For instance, Tincher et al. proposed a method to reduce body coil B_1 field inhomogeneity through three steps [5]. First, the inhomogeneity was modeled using polynomials and least squares approaches. Second, the modeled data was subtracted from the actual image. Finally, the compensated data was rescaled to reduce the B_1 filed inhomogeneity. This method assumes that the inhomogeneity of the RF coil is known from the Biot-Savart law for low frequency operations. The Biot-Savart law was also utilized to optimize the B_1 field by finding an optimal angular placement of the elements of a non-circular birdcage coil [6]. The Biot-Savart law can be very accurate for modeling relatively complex geometries at low frequency, but it is not valid when the coil geometry is a significant fraction of the wavelength. This is particularly true in the ultra high frequency (UHF) range where the electric and magnetic fields become highly coupled.

Simulated annealing has also been used to optimize 16-rung elliptical shielded and unshielded coils [7]. In 1997, Li

* Corresponding author. Tel.: +1-614-293-3046; fax: +1-614-293-7200.
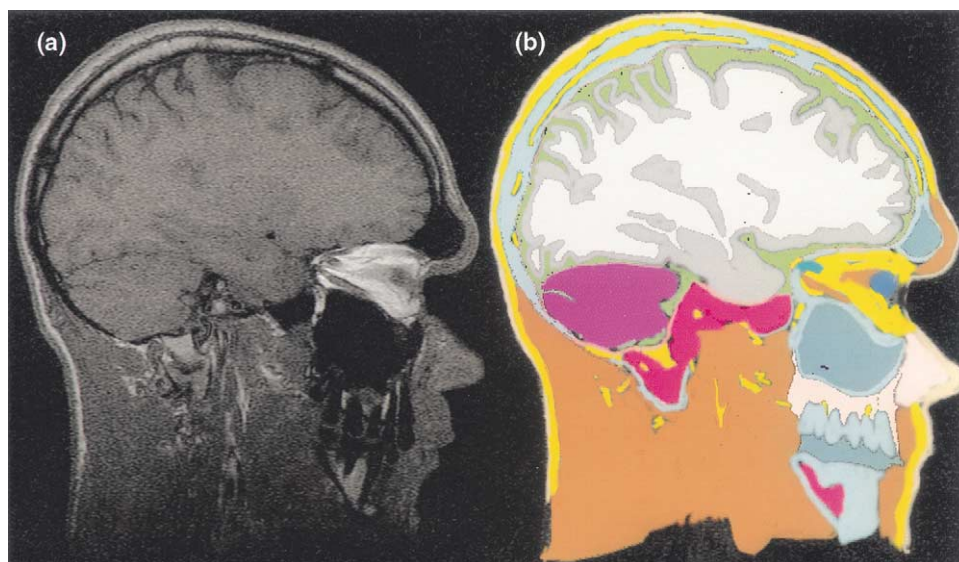*E-mail address:* robitaille.1@osu.edu (P.-M.L. Robitaille).

Fig. 1. An MRI image (a) and its equivalent data slice (b) from the new anatomically detailed human head model.

et al. utilized Ohm's law to obtain the optimum current distribution for an elliptical birdcage coil operating in the linear mode [8]. This technique, however, is only valid when the interactions between the coil and the sample is minimal.

The B_1 field can also be optimized by altering the manner in which the RF coil is driven. Indeed, modification of the excitation source(s) was found to be effective tool in improving B_1 field inhomogeneity, especially for high frequency applications. For instance, interrrung feeding has been successfully used for an eight-capacitor high pass resonator [9]. A four-point excitation with progressive phase shifts of $\pi/2$ [10] has also been applied to a birdcage coil [11] at 85 MHz. More recently, Ibrahim et al. showed the effectiveness of four-port excitation in terms of B_1 field homogeneity and specific absorption rate (SAR) reduction on a high pass birdcage coil loaded with spherical and octagonal phantoms as well as a human head [12].

In this work, the classical finite difference time domain (FDTD) method [13] is applied to explore multiple drive concepts in the TEM resonator [14] for UHF MRI (340 MHz). Input excitations with both variable phase and magnitude are examined. This is accomplished for 2, 3, 4, 6, and 10 excitation ports in a 24-strut TEM resonator loaded with an 18-tissue anatomically detailed human head model. In addition, antenna array concepts are also applied to modify the phase and magnitude of all the 24 possible ports in the 24-strut TEM resonator. By properly exciting each drive port, significantly improved B_1 field homogeneity can be obtained.

2. The human head model

An anatomically detailed human head model was developed from high resolution (0.5 mm by 0.5 mm by 2 mm)

MRI images. The model was constructed with the assistance of a physician who assigned tissue types to pixels in each digital image. A sample of the MRI images (Fig. 1a) and its encoded digital image (Fig. 1b) appear in Fig. 1. In order to obtain a detailed human head structure, 18 tissue types, in additional to air, were identified in the images. These included: blood, bone-cancellous, bone-cortical, cartilage, cerebellum, cornea, cerebro spinal fluid (CSF), dura, fat, gray-matter (GM), mucosa, muscle, nerve, skin, tongue, vitreous-humor, white-matter (WM), and mixed-GM-WM.

In order to generate the FDTD mesh, the manually encoded digital images were processed to remove voids in the data caused by human error in tissue delineation. Erroneous voids were distinguished from true voids (air spaces in the mouth and nasal passages). Erroneous voids were then filled through the assignment of an adjacent tissue type. Automated grid editing software was developed to accomplish this task. Differences from layer to layer (image to image) in the data set were reconciled by re-slicing the data along a different axis and re-examining the data set to identify discontinuities in tissue boundaries. Some interpolation of the data was also required because of the difference in sample spacing within an image and between images. Finally, the corrected image data was output as a single volumetric data set that specifies tissue types at each sample position. The tissue type information stored at each pixel was then used with a look-up-table that provides dielectric constant and conductivity values at any frequency of interest. The large number of tissue types and small pixel size, leads to more accurate results in modeling the internal electromagnetic fields within the biological tissues. This affects both the SAR calculations and the B_1 field distribution in the human head.

The electrical constitutive parameters of these tissue are dispersive, which means that they vary with the frequency

Table 1
Tissue properties of the human head mesh at 340 MHz

Tissue type	$\rho(Kg/m^3)$	ε_r	$\sigma(\mho/m)$
Blood	1060.0	57.50	1.700
Bone-Cancellous	1850.0	21.84	0.209
Bone-Cortical	1850.0	13.91	0.100
Cartilage	1100.0	44.82	0.620
Cerebellum	1040.0	54.40	0.880
Cornea	1050.0	55.40	1.050
CSF	1060.0	69.08	2.300
Dura	1020.0	52.23	0.770
Fat	920.0	5.14	0.040
Gray-Matter	1040.0	57.05	0.839
Mixed-GM-WM	1040.0	49.45	0.669
Mucosa	1020.0	52.69	0.690
Muscle	1040.0	65.57	0.938
Nerve	1040.0	36.80	0.400
Skin	1100.0	43.07	0.540
Tongue	1040.0	59.64	0.800
Vitreous-Humor	1010.0	68.30	1.550
White-Matter	1040.0	41.85	0.499

Fig. 2. An axial slice of the 24-strut TEM resonator loaded with the anatomically detailed human head model in the FDTD grid.

of interest. Thus, within the simulation the appropriate conductivity and the dielectric constant associated with the frequency of interest must be utilized. This is done by tuning the coil to a specified frequency of interest and simultaneously using the constitutive parameters associated with this particular frequency. The density (ρ), relative dielectric constant ($\varepsilon_r = \varepsilon/\varepsilon_0$), and the conductivity (σ) for these tissue types are given at 340 MHz [15] in Table 1.

3. The TEM resonator in the FDTD grid

A theoretical analysis of the TEM resonator is given by the authors [16]. In this work, the RF coil (TEM resonator) and the human head were modeled as a single system with the FDTD method. This approach permits the electromagnetic interactions between the coil, excitation source and the head to be rigorously included. The three-dimensional FDTD model of the TEM resonator consists of 24 coaxial rods. The 2 mm resolution grid is composed of approx. 8 million cells (193*193*193). Due to the large RAM (1–2 Gigabytes) and CPU requirement (up to 135 million unknowns), the Compaq-Dec machine with 64 667 MHz EV7 processors, and 64 Gigabytes of distributed RAM was used for these simulations. A stair-step approximation was used to model the shield and the top and bottom rings of the coil. The coaxial rods were modeled in a similar manner while an FDTD algorithm was used to account for the curvatures of the rods to minimize the errors caused by stair-stepping. Fig. 2 shows an axial slice of the FDTD grid of a 24-strut TEM resonator loaded with the human head model. To account for the RF coil radiation from the top and bottom of the coil, the perfectly matched layer (PML) [17] was used as an absorbing boundary condition.

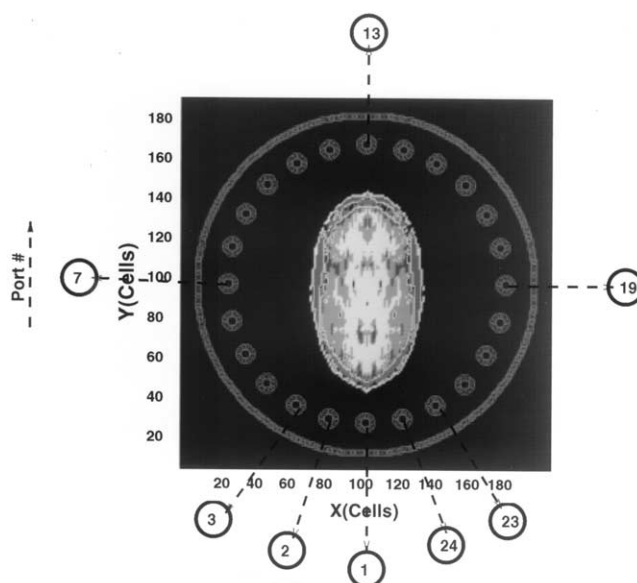The coil was numerically tuned by adjusting the gap between the TEM stubs until mode 1 of the TEM resonator is resonant at the desired frequency of operation. This process was performed while the human head model was present within the coil. A dielectric constant of 2.2 (Teflon) was used for the filler between the inner and the outer rods. Thirteen resonances were observed due to the fact that N-strut TEM resonator has N/2 + 1 TEM modes. It should be noted that theoretically the aforementioned modes are not transverse electromagnetic (TEM) due to two major factors. First, the coil is loaded with the human head. Second, the feed and termination loads introduce perturbations to the fields. These modes are hybrid modes. However, the field distribution associated with one of these hybrid modes correspond closely to the field distribution of mode 1 for the empty resonator. For the purposes of this work, we will also refer to the hybrid mode of interest as mode 1.

4. The variable phase/magnitude excitation system

The use of complex excitation systems is not new in medical applications. For instance, array concepts have been utilized in microwave hyperthermia cancer treatments [18–21]. By exciting sources with appropriate magnitudes and phases, a field distribution can be generated in which the maximum occurs at the tumor. This method is conceptually similar to an antenna array, with the exception that the near field is involved rather than the far field. This concept is also applicable in high frequency MRI. In this case, sources on a volume coil are adjusted in the near field in order to obtain a homogeneous, circularly polarized transverse magnetic (B_1^+) field. In this work, three different feed strategies that involve the phase and the magnitude of the drive points are considered: (1) fixed phase and fixed

(uniform) magnitude (FPFM), (2) variable phase and fixed (uniform) magnitude (VPFM), and (3) variable phase and variable magnitude (VPVM).

Consider Fig. 2 and FPFM excitation. Conventional two-port quadrature excitation was utilized. This includes back of the head quadrature excitation (ports 4 and 22), side of the head quadrature excitation (ports 4 and 10), and front of the head quadrature excitation (ports 10 and 16). In these cases, the drive is split into two parts. A $\pi/2$ phase shift is applied to one part which is then fed to the first port while the other drive is fed directly to the other port without adding a phase shift. The three-port system uses ports 1, 17, and 9 or 13, 5, and 21 in Fig. 2. The drive is split into three parts which comprise 0, $4\pi/3$, and $-4\pi/3$ phase shifts. These, in turn, are fed to the three drive points.

The four-port drive utilizes the 4 ports used for two-port quadrature excitation: 22, 16, 10, and 4. In this case, $\pi/4$, $3\pi/4$, $-3\pi/4$, and $-\pi/4$ phase shifts are applied on each segment of the incoming RF. These segments are then fed to ports 22, 16, 10, and 4, respectively. The six-port system combines the 2 three-port drives described above. Phase shifts of 0, $\pi/3$, $2\pi/3$, π, $-2\pi/3$, and $-\pi/3$ phase shifts are applied to ports 1, 21, 17, 13, 9, and 5 respectively. The ten-port drive combines the ports of the four-port and the six-port systems with the same phase shifts described for these configurations.

The VPFM and the VPVM driving schemes were used in the three-port, four-port, six-port, and ten-port systems using the drive points previously described. For these two drive systems, the phase or (phase and magnitude) of each excitation element was/were adjusted to produce an optimum uniform circularly polarized B_1 field.

In addition to the drive systems described above, a 24-port system was obtained by exciting all 24 struts of the resonator. FPFM excitation was used by applying progressive $\pi/12$ phase shifts on each port starting from port 24 (Fig. 2) and proceeding in a counter-clock wise direction. VPFM and VPVM excitations were also examined.

The VPFM and the VPVM systems are developed as follows. The coil is first excited at a specified port. The excitation is performed with a specified gap size between the inner rods of each coaxial line, and a specified dielectric constant of the filler between the inner and outer rods. Conductivity and dielectric constant parameters, in our case the values at 340 MHz, are assigned to the human head tissues. This process (excitation) is accomplished while the TEM resonator and the human head are modeled as a single system. Time domain data is collected and a Fourier transformation is applied to find the resonance frequency of mode 1. If the resonance frequency of mode 1 lies at the frequency of interest (340 MHz), the code is re-executed and the frequency domain solution of the field is obtained at 340 MHz. If the previous condition is not satisfied, the entire process described above is performed with a different gap size between the inner rods of each coaxial line.

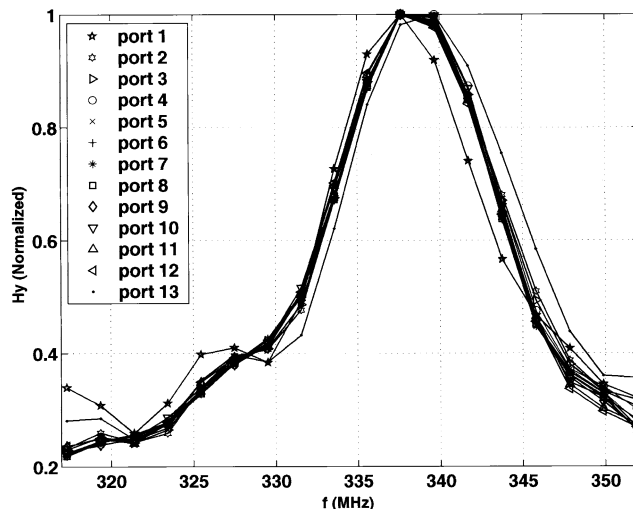The previous process is repeated for all the excitation

Fig. 3. Frequency responses obtained using the FDTD model at one point inside the human head model loaded in a 24-strut TEM resonator. The excitations used ports 1–13 and the frequency response of every excitation was collected at the specified point. The resonance frequency of TEM mode 1 lies at approximately 340 MHz regardless of which port was excited. Note that Teflon was used to fill all the coaxial lines for all cases.

ports of interest (3, 4, 6, 10, or 24 ports). Super position of all the solutions obtained at all the excitation ports (with the desired phase or phase and magnitude) was then applied to compute the total response (field distribution). Using a numerical optimization process, the phase or the phase and magnitude of the excitation ports was/were optimized such that an optimum B_1^+ field (lowest standard deviation of the field distribution) was obtained in a particular slice of interest in the head. This optimization process was computationally expensive due to the number of parameters which are varied to obtain an optimum B_1^+ field distribution. For instance, a VPVM 24-port system involves the variance of 47 parameters (23 phase shifts and 24 magnitudes). In addition to the large number of variable parameters, the optimization process is nonlinear, which significantly increases the computational resources required.

In order to ensure the validity of the proposed 24-port system, the resonance frequency of mode 1 must approximately lie at same location (340 MHz) regardless of which drive port is used for excitation. Note that the same material has to be used to fill all the coaxial lines, and the gap between the tuning rods within all the coaxial lines must be fixed for all (24) excitations. For the simulations shown here, these two conditions were satisfied. Frequency responses obtained using the classical FDTD model at one point inside the head loaded 24-strut TEM resonator are shown in Fig. 3. The excitations were done using ports 1–13, and the frequency response of every excitation was collected at the specified point. It is clear that the resonance frequency of mode 1 lies at approximately 340 MHz regardless of which port is excited. The bandwidth is also similar in all the thirteen cases. Note that ports 14 to 24 are reciprocal to ports 12 to 2.

5. Experimental confirmation

Experiments were performed to confirm the model described above. Images were acquired on an 8.0T/80 cm superconducting magnet (Magnex Scientific, Abingdon, UK). The scanner was equipped with a BRUKER AVANCE console (Bruker, Billerica, MA, USA). All human studies were conducted under an investigational device exemption (IDE) granted by the Food and Drug Administration (FDA). Studies were also monitored by the IRB committee of The Ohio State University. Prior to image acquisition, the subject was asked to lie in a supine position on a movable cantilevered patient table. A 16-strut TEM resonator was then positioned over the subject's head such that the face of the RF coil was aligned with the chin of the subject (full insertion). The RF coil was tuned to 340 MHz as monitored on each of two drive points connected in quadrature. The locations of the drive points were symmetrically placed, roughly behind the ears. The patient was then advanced to the scan position while remaining on the table and without removal of the RF coil. Low flip angle (30°) gradient echo human images were then acquired using the following parameters: TR = 500 msec, TE = 8.1 msec, FOV = 20 cm, matrix = 256 × 256, number of slices = 10, receiver bandwidth = 50 kHz, excitation pulse = 4 msec Gaussian.

For validation purposes, a simulation of a 16-strut TEM resonator loaded with the human head model was performed at 340 MHz. The bottom ring of the FDTD model of the TEM resonator was aligned with the chin of the anatomically detailed human head mesh. The numerical model of the coil had the same geometry and dimensions as the coil used in experiment. The model used 2-port quadrature excitation where the drive ports were positioned behind the head. Fig. 4 displays an axial slice of the calculated B_1^+ field using the FDTD model at 340 MHz (a) and the low flip angle gradient echo image obtained at 8 Tesla (b). It is apparent that the shading and brightness of the MRI image are similar to the B_1^+ field distribution obtained using the FDTD calculations.

6. Distribution of the B_1^+ field

Distributions of the B_1^+ field are displayed in Fig. 5. Axial slices were obtained by using the FDTD model with 24-strut TEM resonator driven by a FPFM excitation at 340 MHz. Figs. 5a, 5b, and 5c correspond to the B_1^+ field obtained with 2-port excitation at ports 4 and 22 (5a), 4 and 10 (5b), and 10 and 16 (5c). Figs. 5d, and 5e correspond to the B_1^+ field with 3-port excitation and utilizing ports 1, 17, and 9 (5d), and 13, 5, and 21 (5e). Figs. 5f, 5g, and 5h correspond to the results obtained with 4-port (5f), 6-port (5g), and 10-port (5h) excitations. The ports used for these excitations are described in Section 4. The standard devia-
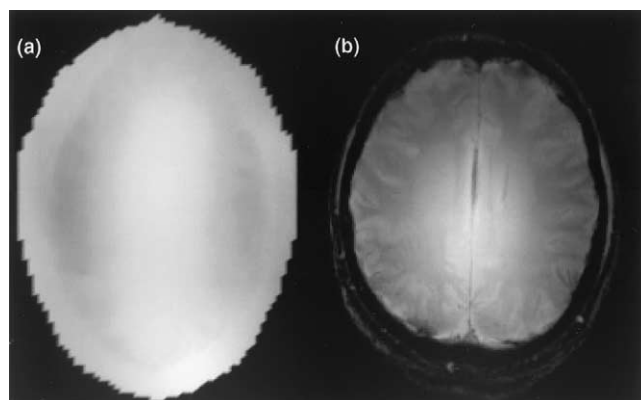

Fig. 4. (4a) is the calculated circularly polarized component of the B_1 (B_1^+) field inside a 16-strut TEM resonator operating under 2-port (behind the head) quadrature excitation. The results were obtained using the FDTD model at 340 MHz (8 Tesla). (4b) is a low flip angle (30°) gradient echo human image of a 16-strut TEM resonator that has the same geometry, dimensions, and excitation as the model used in Fig. 4a. The image parameters are: TR = 500 msec, TE = 8.1 msec, FOV = 20 cm, matrix = 256 × 256, number of slices = 10, receiver bandwidth = 50 kHz, excitation pulse = 4 msec Gaussian.

tion (SD) values of the B_1^+ field in these axial slices are shown in Table 2.

These results indicate that increasing the number of excitation ports improves the homogeneity of the B_1^+ field until a minimal SD value = 0.1306 (Table 2) was obtained using 6-port excitation. Increasing the number of ports to 10 and then to 24, did not produce further decreases in SD. In fact, the SD value increased to 0.1333 for 10-port excitation and then it slightly decreased to 0.1321 using 24-port excitation (Table 2). Therefore, a fixed-phase progression on the ports is not optimal for producing homogeneous circularly polarized fields. This is because the EM fields associated with the particular mode of operation are neither transverse electromagnetic (TEM) nor linearly polarized (using 1-port excitation). The previous two facts are true since (a) the coil dimensions constitute a large fraction of the operating wavelength and (b) the coil load is electrically large, inhomogeneous, lossy, asymmetric, irregular in shape. Such conditions make it impossible to generate a pure TEM mode or a pure linear polarization in a coil loaded with a human head operating at UHFMRI (>7 Tesla).

Fig. 6 displays the B_1^+ field distribution inside the human head model using the FDTD model. Results were calculated within a 24-strut TEM resonator using VPFM (6 a–e) and VPVM (6 f–j) excitations at 340 MHz. The results were obtained using 3-port (6a and 6f) and (6b and 6g), 4-port (6c and 6h), 6-port (6d and 6i), and 10-port (6e and 6j) systems. Ports 1, 17, and 9 were used in Figs. 6a and 6f and ports 13, 5, and 21 were used in Figs. 6b and 6g. The ports used for the 4-port, 6-port, and 10-port systems were the same as those used in Fig. 5. Table 2 displays the SD values of the B_1^+ field using the aforementioned excitations.

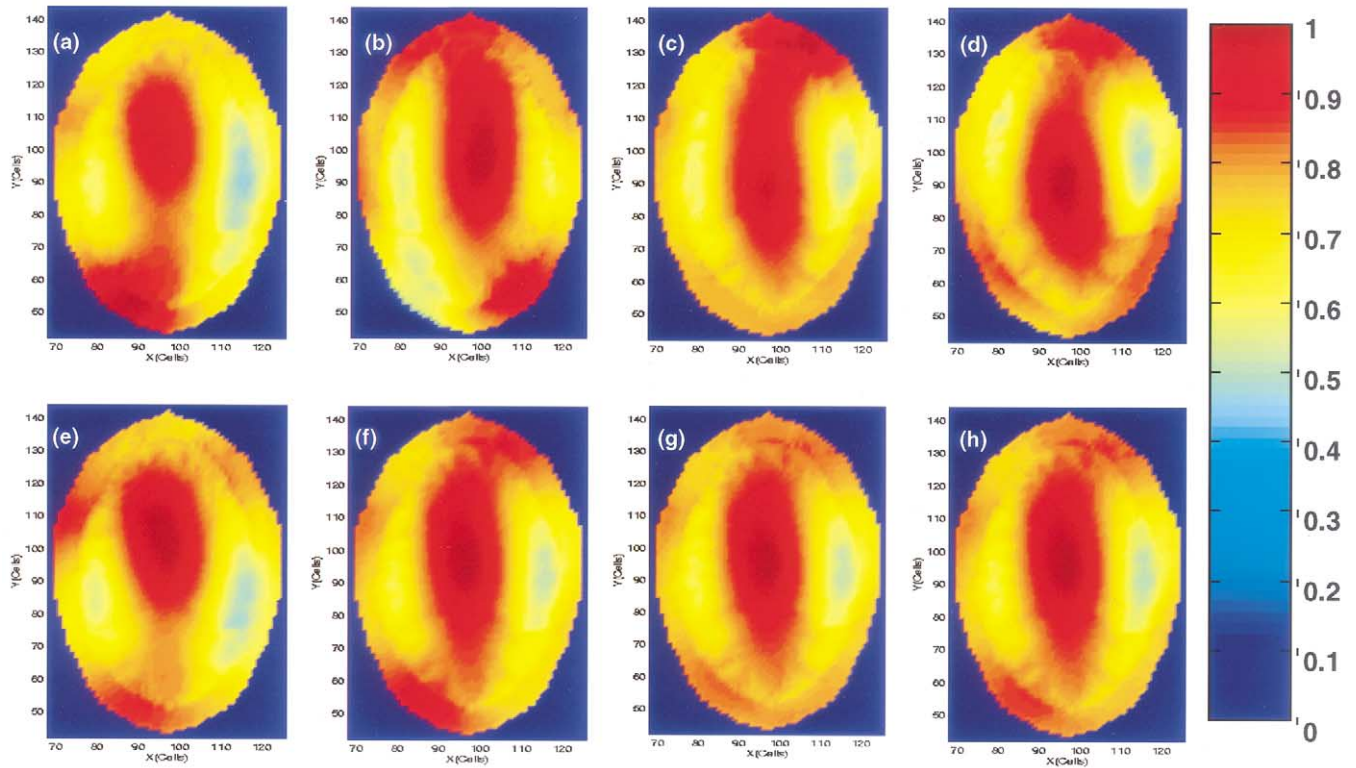Unlike the FPFM excitation, SD values for VPFM and

Fig. 5. Axial slices of the B_1^+ field distribution inside the human head model at 340 MHz. Results were obtained with a 24-strut TEM resonator using fixed-phase and fixed-magnitude excitation. Figs. 5a–c correspond to the B_1^+ field with 2-port excitation, utilizing ports 4 and 22 (5a), 4 and 10 (5b), and 10 and 16 (5c). Figs. 5d, and 5e correspond to the B_1^+ field with 3-port excitation and utilizing ports 1, 17, and 9 (5d), and 13, 5, and 21 (5e). Figs. 5f–h correspond to the results obtained with 4-port (5f), 6-port (5g), and 10-port (5h) excitations. The ports used were 4, 22, 16, and 10 for 4-port excitation and 1, 17, 9, 13, 5, and 21 for 6-port excitation; all of the previous ports were used for 10-port excitation. The ports identification numbers are given in Fig. 2.

VPVM monotonically decrease with increasing the number of excitation ports and by varying the phase or the phase and magnitude of each excitation port (Table 2). Table 2 shows that the SD value improved from 0.1361 using 3-port VPFM excitation to 0.0888 using 10-port VPVM excitation. These findings show that the EM interactions between the coil and the tissue in general and the interactions between the excitation source(s) and the tissue in particular dominate the B_1^+ field distribution in the head.

Based on the previous results, it is clear that one can

Table 2
Calculated standard deviation values of the circularly polarized component of the B_1 (B_1^+) field in axial slices through the human head model. The calculations were done using the FDTD model where the mean value of the B_1^+) field in the slice is set to 1.

Excitation type								
Fixed phase and fixed magnitude			Variable phase and fixed magnitude			Variable phase and variable magnitude		
# of ports	Ports used*	Standard deviation	# of ports	Ports used*	Standard deviation	# of ports	Ports used*	Standard deviation
	4,22	0.1617	NA	NA	NA	NA	NA	NA
2	4,10	0.1538	NA	NA	NA	NA	NA	NA
	10,16	0.1421	NA	NA	NA	NA	NA	NA
3	1, 17,9	0.1423	3	1,7,9	0.1361	3	1,17,9	0.1277
	13,5,21	0.1524		13,5,21	0.1328		13,5,21	0.1323
4	22,16, 10,4	0.1395	4	22,16, 10,4	0.1273	4	22,16, 10,4	0.1196
6	1,17,9, 13,5,21	0.1306	6	1, 17, 9, 13, 5, 21	0.1158	6	1, 17, 9, 13, 5, 21	0.0965
10	22, 16, 10, 4, 1, 1, 17, 9, 13, 5, 21	0.1333	10	22, 16, 10, 4, 1, 17, 9, 13, 5, 21	0.1026	10	22, 16, 10, 4, 1, 17, 9, 13, 5, 21	0.0888
24	All ports	0.1321	24	All ports	0.0814	24	All ports	0.0685

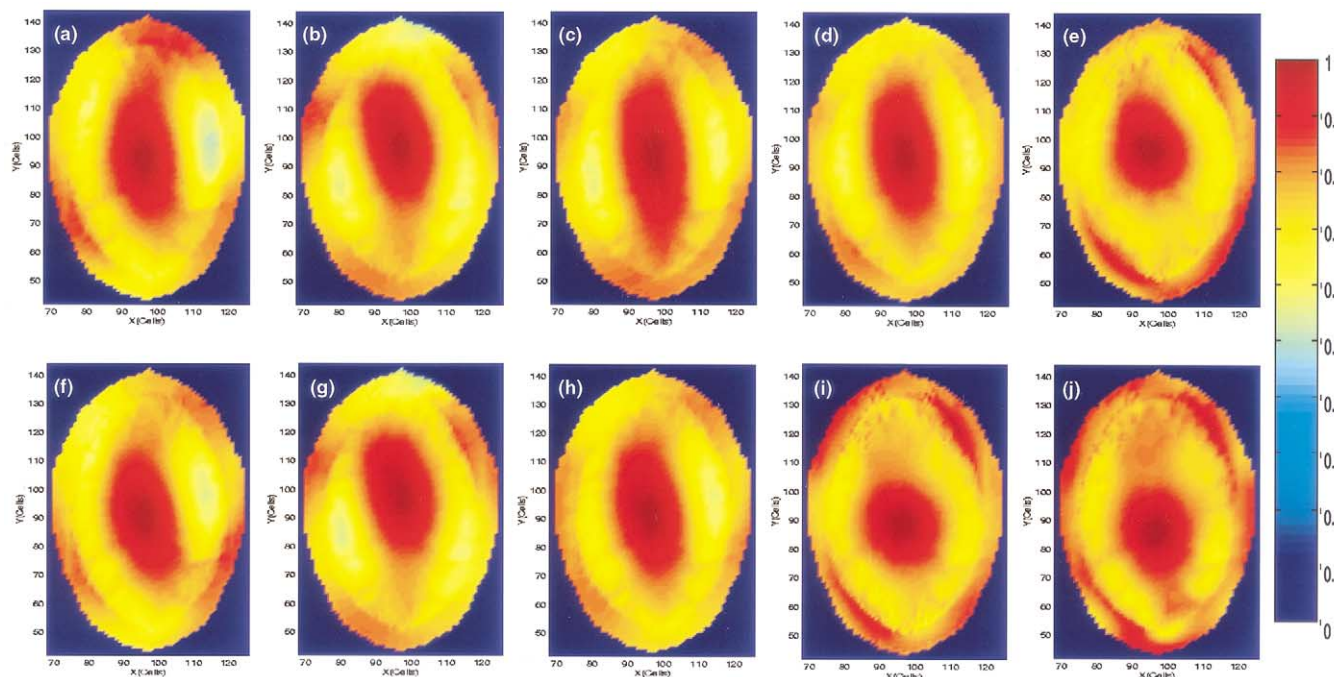* The ports identification numbers are given in Figure 2.

Fig. 6. Axial slices of the B_1^+ field distribution inside the human head model. Results were obtained with a 24-strut TEM resonator using variable-phase and fixed-magnitude (6a–e) and variable phase-variable magnitude (6f–j) excitations at 340 MHz. The figures correspond to 3-port (6a and 6f) and (6b and 6g), 4-port (6c and 6h), 6-port (6d and 6i), and 10-port (6e and 6j) systems. Ports 1, 17, and 9 were used in Figs. 6a and 6f and ports 13, 5, and 21 were used in Figs. 6b and 6g. The ports used for the 4-port, 6-port, and 10-port systems are described in Fig. 2.

further improve the homogeneity of B_1^+ field distribution by driving all the coaxial rods of the coil. Fig. 8 shows the B_1^+ field distribution inside the human head model using 24-port FPFM (8b), VPFM (8c), and VPVM (8d) excitations. In Fig. 8a, a 24-strut 2-port FPFM excitation using struts 4 and 22 (back of the head), is illustrated for comparison. Table 2 provides the SD values of the B_1^+ field distribution for the 2-port and 24-port excitation systems. It is observed that the SD of the VPVM 24-port system is equal to 0.0685, almost a 2-fold improvement over the 24-port FPFM system and nearly 2.5-fold better than the

two port system (Table 2). The VPVM solution is presented in Table 3.

The development of the 24-port VPVM system would require 24 phased-locked transmitter/receiver channels. These transceivers must be designed such that the phase and the magnitude of each channel can be controlled independently of all the other (23) channels. Because of different head sizes, it is necessary to create a database of the phases (VPFM) or the phases and magnitudes (FVFM) of the excitation ports where the values of these parameters are computationally calculated for different head models using
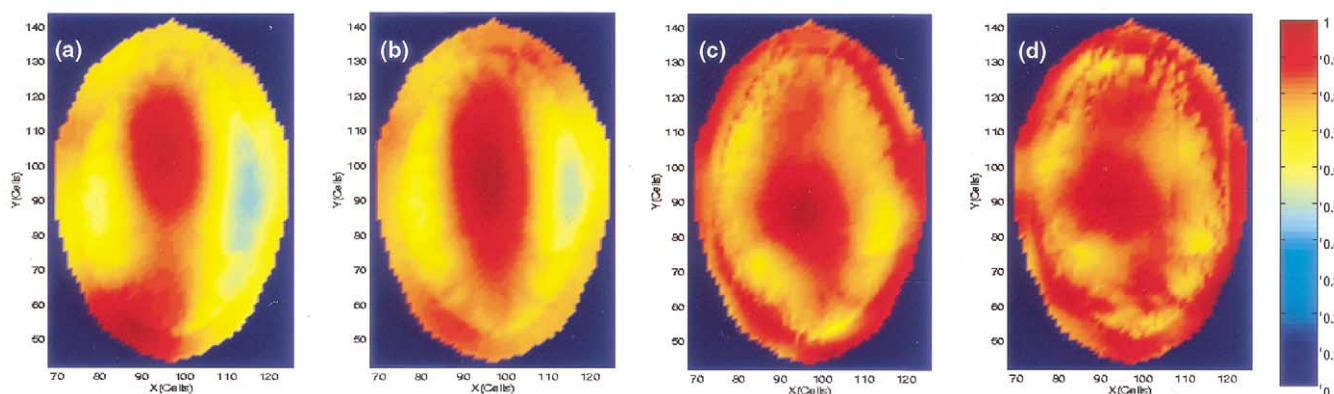

Fig. 7. The calculated B_1^+ field distribution inside the human head model at 340 MHz. The human head model was loaded in a 24-strut TEM resonator excited at ports 4 and 22 (7a) and at all the possible ports (24) (7b–d). The results are presented for fixed-phase & fixed-magnitude (7a and 7b), variable-phase & fixed-magnitude (7c) and variable-phase & variable-magnitude (7d) systems.

Table 3
The relative phases and magnitudes of excitation ports 1–24 (Figure 2) required to obtain a standard deviation value equal to 0.0685 of the B_1^+ field in an axial slice through the human head model at 340 MHz[a]

Port identification number*

Relative phase (degrees) Relative magnitude

1		2		3		4	
0.000	0.001	79.18	0.050	240.49	0.055	359.89	0.145
5		**6**		**7**		**8**	
174.50	0.212	44.60	0.105	233.49	0.070	346.89	0.219
9		**10**		**11**		**12**	
180.00	0.270	15.07	0.279	206.92	0.335	54.36	0.220
13		**14**		**15**		**16**	
318.12	0.096	19.21	0.083	182.48	0.107	237.20	0.023
17		**18**		**19**		**20**	
180.07	0.121	345.04	0.164	69.63	0.057	181.40	0.042
21		**22**		**23**		**24**	
48.07	0.030	16.90	0.001	240.40	0.058	276.49	0.024

* The ports identification numbers are given in Figure 2.

[a] These values correspond to the variable-phase&variable-magnitude 24-port system used to obtain the results of Figure 7d.

the FDTD technique described above. These sets of phases and magnitudes could then be applied to the 24-channel system such that an optimal B_1^+ field distribution is obtained.

The results in this work provide conclusive evidences that at 340 MHz, the B_1^+ field distribution inside the human head is dominated by the interactions between the head, coil, and excitation source rather than the head by itself. As such, the limitations on achieving a homogeneous MRI image at ultra high field are due to sample-coil interactions and technological difficulties and not dominated by fundamental physical phenomenon such as "dielectric resonances" [22–24].

7. Summary and conclusions

When performing computational electromagnetic simulations of high frequency MRI applications, an accurate high-resolution human head model is essential to obtain realistic estimates of the internal electromagnetic fields within the tissue. In this work, through the use of the classical finite difference time domain (FDTD) method, a complete analysis of the TEM resonator loaded with a newly developed anatomically detailed human head model was presented at 8 Tesla (340 MHz). The 2 mm × 2 mm × 2 mm FDTD mesh data of the head were obtained from high resolution (0.5 mm × 0.5 mm × 2 mm) MRI images. The classical FDTD model accounts for electromagnetic interactions among the coil, excitation source, and head. This was done by treating the TEM resonator and the human head as a single system in all the steps of the model including excitation and numerical tuning. The numerical results were validated with low flip angle gradient echo MRI im-

ages of the head at 8 Tesla. Good agreement was obtained between the measurements and the FDTD calculations.

The B_1 field homogeneity was examined inside a 24-strut TEM resonator at 340 MHz using different excitations techniques namely, fixed-phase and fixed-magnitude (FVFM), variable-phase and fixed-magnitude (VPFM), and variable-phase and variable-magnitude (VPVM) systems. This was accomplished through the use of multi-port (2, 3, 4, 6, and 10 ports) excitation. It was observed that the resonance frequency and bandwidth of the mode of interest were consistent for each excitation port, which implies a resonance of the entire system as desired. In addition, a full multiple drive concept was utilized to drive all the possible (24) struts of the coil. The optimization criteria of the phases or the phases and magnitudes of the drive ports was the minimization of the standard deviation of the circularly polarized component of the B_1 (B_1^+) field.

In axial slices through the brain, a significant improvement in the B_1^+ field homogeneity was obtained by varying the phase (or the phase and magnitude) of each excitation source beyond a linear phase progression. For instance, the standard deviation of the B_1^+ field decreased from 0.1617 using conventional back of the head quadrature excitation to 0.0685 (2.5 fold improvement) using VPVM 24-port excitation. Based on these results it is concluded that (1) highly homogeneous MRI images at ultra high field are physically feasible, (2) electromagnetic fields within the head are dominated by the interactions between the coil, excitation source(s) and the head.

References

[1] Ibrahim TS, Lee R, Abduljalil AM, Baertlein BA, Robitaille P-ML. Dielectric resonances and B_1 field inhomogeneity in UHFMRI: computational analysis and experimental findings. Magn Reson Imaging 2001;19:219–26.

[2] Kangarlu A, Baertlein BA, Lee R, Ibrahim TS, Abduljalil AM, Yang L, Robitaille P-ML. An analysis of the dielectric resonance phenomenon in ultra high field magnetic resonance imaging. J Comp Assist Tomogr 1999;23:821–31.

[3] Ibrahim TS, Lee R, Baertlein BA, Kangarlu A, Robitaille P-ML. On the physical feasibility of achieving linear polarization at high-field: a study of the birdcage coil. In Book of abstracts. in Book of abstracts: Seventh Annual Meeting of International Society of Magnetic Resonance in Medicine, Vol. 1. Philadelphia, Pennsylvania: ISMRM, 1999. p. 2058.

[4] Ibrahim TS, Lee R, Baertlein BA, Yu Y, Robitaille P-ML. Computational analysis of the high pass birdcage resonator: Finite difference

time domain simulations for high-field MRI. Magn Reson Imaging 2000;18:835–43.

[5] Tincher M, Meger CR, Gupta R, Williams DM. Polynomial modeling and reduction of RF body coil spatial inhomogeneity in MRI. IEEE Trans on Medical Imaging 1993;12:361–665.

[6] Riauka TA, De Zanche NF, Thompson R, Vermeulen FE, Capjack CE, Allen PS. A numerical approach to non-circular birdcage RF coil optimization: Verification with a fourth-order coil. Magn Reson Med 1999;41:1180–8.

[7] Forbes LK, Crozier S, Doddrell DM. An analysis and optimization of RF probes used in magnetic resonance imaging. Measurement in Science and Technology 1996;7:1281–90.

[8] Li SL, Collins CM, Dardzinski BJ, Chin C-L, Smith MB. A method to create an optimum current distribution and homogeneous B_1 field for elliptical birdcage coils. Magn Reson Med 1997;37:600–8.

[9] Crozier S, Luescher K, Forbes LK, Doddrell DM. Optimized small bore high-pass resonator designs. J Magn Reson Series B 1995;109:1–11.

[10] Bridges JF. Cavity resonator with improved magnetic field uniformity for high frequency operation and reduced dielectric heating in NMR imaging devices. U.S. Patent 4751464; 1988.

[11] Hayes EC, Edelstein WA, Schenck JF, Mueller OM, Eash M. An efficient highly homogeneous radiofrequency coil for whole-body NMR imaging at 1.5 T. J Magn Reson 1985;63:622–828.

[12] Ibrahim TS, Lee R, Baertlein BA, Kangarlu A, Robitaille P-ML. Application of finite difference time domain method for the design of birdcage RF head coils using multi-port excitations. Magn Reson Imaging 2000;18:733–42.

[13] Yee KS. Numerical solution of initial boundary value problems involving Maxwell's equations in isotropic media. IEEE Trans Antennas Propagation 1966;AP-14:302–7.

[14] Vaughan JT, Hetherington HP, Otu JO, Pan JW, Pohost JM. High frequency volume coils for clinical NMR imaging and spectroscopy. Magn Reson Med 1994;32:206–18.

[15] Gabriel C. Compilation of dielectric properties of body tissues at RF and microwave frequencies. AL/OE-TR-1996-0037 1996.

[16] Baertlein BA, Ozbay O, Ibrahim TS, Lee R, Kangarlu A, Robitaille P-ML. Theoretical model for an MRI radio frequency resonator. IEEE Trans Biomed Engineer 2000;47:535–46.

[17] Berenger J. A perfectly matched layer for the absorption of electromagnetic waves. Journal of Computational Physics 1994;114:185–200.

[18] Chen J-Y, Gandhi OP. Numerical simulation of annular-phased arrays of dipoles for hyperthermia of deep-seated tumors. IEEE Trans Biomed Engineer 1992;39:209–16.

[19] Lynch DR, Paulsen KD, Strohbehn JW. Finite element solution of Maxwell's equations for hyperthermia treatment planning. J Comp Physics 1990;58:246–69.

[20] Wang C-Q JT, Gandhi OP. Numerical simulation of annular phased arrays for anatomically based models using the FDTD method. IEEE Trans on Microwave Theory and Techniques 1989;37:118–26.

[21] Chowdhury DQ, Hill SC. Numerical optimization of 3-D SAR distributions in cylindrical models for electromagnetic hyperthermia. IEEE Trans on Biomedical Eng 1991;38:1246–55.

[22] Roschmann P. Radiofrequency penetration and absorption in the human body: Limitations to high-field whole-body nuclear magnetic resonance imaging. Med Phys 1987;14:922–31.

[23] Bomsdorf H, Helzel T, Kunz D, Roschmann P, Tschendel O, Wieland J. Spectroscopy and imaging with a 4 Tesla whole-body MR system. NMR Biomed 1988;1:151–8.

[24] Jin JM, Chen J, Chew WC, Gan H, Magin RL, Dimbylow PJ. Computation of electromagnetic fields for high-frequency magnetic resonance imaging applications. Physics Med Biology 1996;41:2719–38.